Inorganic Chemistry

Article

pubs.acs.org/IC

Molecular Dynamics Simulation of the Solid-State Topochemical Polymerization of S_2N_2

Teemu T. Takaluoma,[†] Kari Laasonen,[‡] and Risto S. Laitinen*[,†]

[†]Department of Chemistry, University of Oulu, P.O. 3000, FI-90014 Oulu, Finland

[‡]School of Chemical Technology and COMP Center of Excellence, Aalto University, P.O. Box 16100, FI-00076 Aalto, Espoo, Finland

Supporting Information

ABSTRACT: Molecular dynamics simulations of the solid-state topochemical polymerization of four-membered S_2N_2 rings to $(SN)_x$ have been presented by involving DFT methods and periodic functions. Isotropic pressure compression and a slightly elevated temperature have been applied to lower the activation barriers and to increase the rate of the reaction to be within the framework of MD simulations. The polymer formation is initiated by the cleavage of one bond in one S_2N_2 ring with a virtually instantaneous attack of the fragment thus formed on the neighboring ring. The energetically most-favored reaction then quickly propagates along *a* axis throughout the lattice. The structures of the polymer chains are in good agreement with that observed experimentally in the crystal structure determination, but there is less long-range order between the neighboring chains. Upon polymerization the packing of the molecules changes from the herringbone structure of the S_2N_2 lattice to a layered structure in the $(SN)_x$ lattice. While not the same, the simulated and experimental packing changes bear a qualitative similarity. The simulated polymerization was also observed to propagate along *c* axis in addition to *a* axis, but these side effects generally disappear toward the end of the simulations. In some cases, the polymers propagating simultaneously in both *a* and *c* axis directions persist at the end of the simulation resulting in a complicated network of sulfur−nitrogen chains. This finds experimental support in the observation of several polymorphs $(SN)_x$ with severe disorder in the lattice.

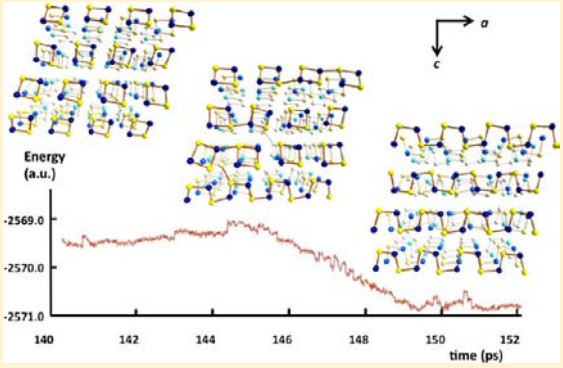

INTRODUCTION

Polymeric sulfur nitride $(SN)_x$ is one of the most fascinating compounds that has emerged during the recent decades. The discovery in the 1970s that it is a metallic conductor and that it becomes superconducting below 0.33 K has boosted research activity in the synthetic and structural investigations of sulfur−nitrogen compounds.[1−5] $(SN)_x$ is generally prepared by slow solid-state polymerization of S_2N_2, which is generated by thermal decomposition of S_4N_4 over a silver wool catalyst.[6] The reaction has been shown to afford monoclinic β-$(SN)_x$ (90%) together with a small amount of orthorhombic α-$(SN)_x$ (10%).[7] A polymeric powder has also been prepared by the addition of trimethylsilyl azide to $(NSCl_3)$ in acetonitrile,[8,9] and by photopolymerization of S_2N_2 in THF.[10] Thin films of $(SN)_x$ have been produced on plastic or metal surfaces by the electroreduction of $[S_5N_5]^+$ salts.[11] Rapid polymerization has recently been observed to take place within the channels of a zeolite host by using a porous framework with the appropriate dimensions to accommodate S_2N_2 and $(SN)_x$.[12]

Polymeric sulfur nitride is a shiny metallic solid consisting of highly oriented parallel fibers. The single crystal X-ray structure of β-$(SN)_x$ reveals an almost-planar *cis*, *trans* polymer.[13] The polymer exhibits anisotropic electrical conductivity at room temperature and becomes superconducting below liquid helium temperature. The conductivity across the fibers is much smaller than along the strands.

The electric properties of $(SN)_x$ have resulted in several patents and reports of the use of the material in a wide variety of solid-state devices such as solar cells, light emitting diodes, or as electrodes (for a review, see ref 3). One potential application of the polymerization process of S_2N_2 is the rapid imaging of latent fingerprints based on their interaction with S_2N_2 vapor to give a visible image because of the formation of the blue-black polymer $(SN)_x$.[14,15] The image is formed rapidly on a variety of surfaces such as paper, pottery, glass, and textiles, and is therefore of interest in forensic science.

The early models for the topochemical polymerization process have been reviewed by Banister and Gorrell.[3] The generally accepted mechanism is based on the suggestion by Baughman et al.[16−19] that the polymerization occurs via one-point ring cleavage involving the minimized root-mean-square displacements of the atoms (see Figure 1). This mechanism also explains the origin of the structural defects, which have been observed in crystalline $(SN)_x$ (see Scheme 1). The time-resolved X-ray diffraction study by Müller et al.[7] is consistent

Received: February 1, 2013
Published: March 29, 2013

   dx.doi.org/10.1021/ic400273p | *Inorg. Chem.* 2013, 52, 4648−4657

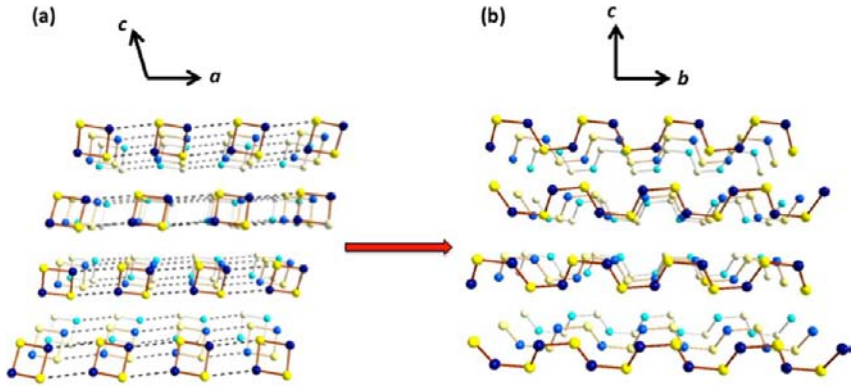

Figure 1. Comparison of the crystal lattices of (a) S_2N_2 and (b) $(SN)_x$ (adapted and redrawn from ref 13). The *b* axis in part a is directed away from the reader and the *a* axis in part b is directed toward the reader. Sulfur atoms are indicated by yellow spheres and nitrogen atoms by blue spheres.

Scheme 1. Four Alternative Routes of Equal Probability for the Linear Polymerization of Two Neighboring Rows of S_2N_2

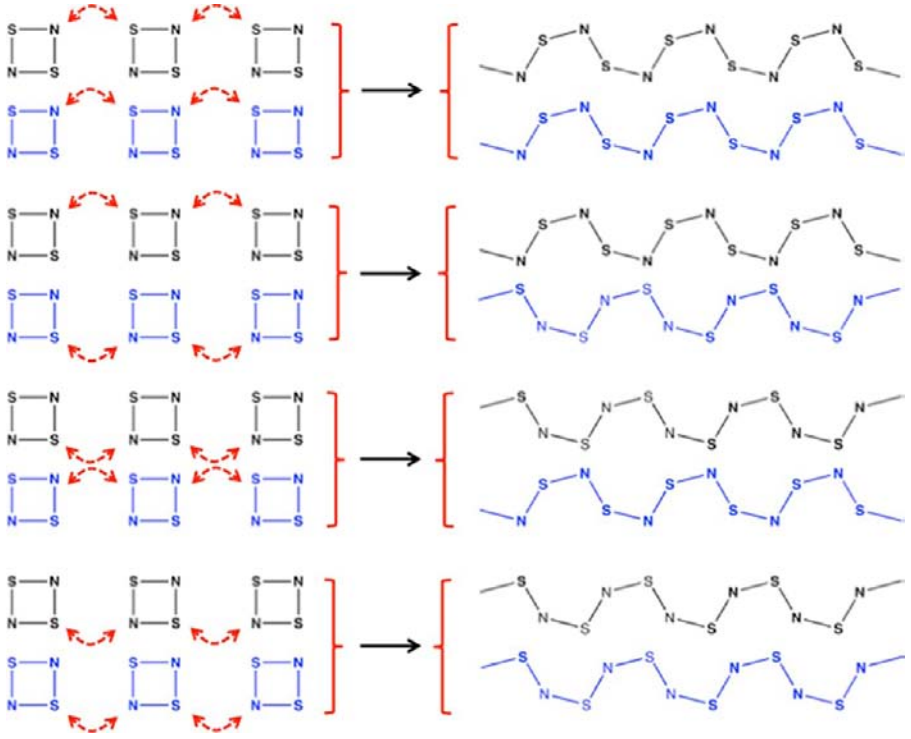

with this mechanism. As Banister and Gorrell[3] have pointed out, the formation of α-$(SN)_x$ upon polymerization may well explain the disorder reported in many early structural studies. It has more recently been proposed that the polymerization mechanism involves excitation of the square planar singlet S_2N_2 molecule to the triplet surface, followed by puckering of the triplet species and polymerization in a direction approximately perpendicular to the plane of S_2N_2 rings.[20]

Using FTIR spectroscopy, Kanazawa et al.[21,22] inferred that the polymerization is autocatalytic with the rate dependent on temperature and crystal size. The polymerization was initiated either by photoactivation or thermal activation.[22] Love and Labes[23] observed that during the polymerization the reaction intermediates exhibited ESR signals, which vanished when the polymerization was complete. This indicates the presence of radicals among the reaction intermediates.

In this work we model the solid-state polymerization of S_2N_2 by combining DFT computations involving periodic functions with molecular dynamics calculations. Since these simulations involve picosecond time frame, whereas the actual polymerization of S_2N_2 is very slow taking several hours at room temperature, we utilized high external pressure in the calculations to increase the reaction rate. The objectives were to determine if the topochemical polymerization of the single crystal of S_2N_2 to $(SN)_x$ can be modeled under these conditions, and to establish the pathway of the polymerization and the final structure of the crystalline polymer.

Application of high pressure on molecular liquids and solids has a significant effect on their volumes, electronic properties, and reactivity.[24−26] Alternative reaction paths may appear, and reactions can either be kinetically accelerated or inhibited.[24] Molecular materials are highly compressible, and even relatively mild pressures of 1 GPa can result in 25% reduction in volume. At high pressures the intermolecular distances shorten and the repulsive intermolecular interactions may be in the comparable magnitude range with attractive intramolecular interactions.

dx.doi.org/10.1021/ic400273p | *Inorg. Chem.* 2013, 52, 4648−4657

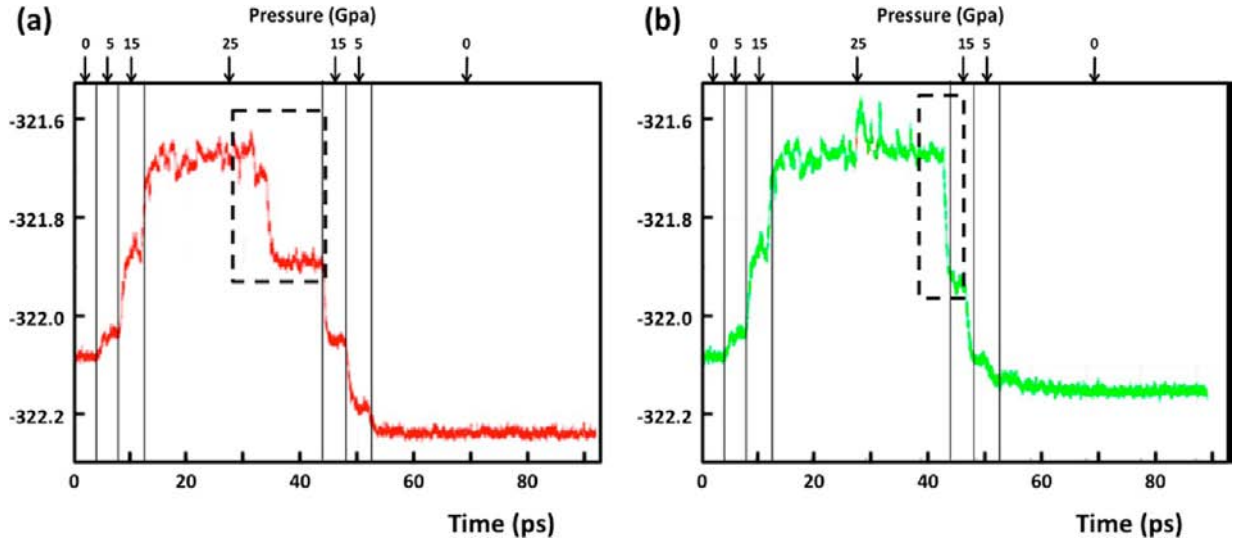

Figure 2. Potential energy evolution during the $S_2N_2 \rightarrow (SN)_x$ polymerization simulated on the *221* supercell at 300 K. Vertical lines designate the times where pressure is changed in the simulation. The time period during which the polymerization of S_2N_2 took place is indicated by a black dashed rectangle. (a) The energy profile of the energetically most favorable polymerization along the *a* axis is shown in red. (b) The energy profile of one of the alternative routes leading to the formation of a complicated polymer network.

Under these conditions, the system can therefore become thermodynamically unstable resulting in the rearrangement of the molecular packing or may even lead to topotactic chemical reactions.[25]

The effect of pressure on the solid-state reactions is exemplified by the polymerization of ethyne,[25,27] which has been modeled by molecular dynamics solid-state simulation at the BP86 level of theory.[28] The simulation was carried out on the supercells containing 16 or 32 C_2H_2 molecules. A rapid polymerization was observed at a temperature of 400 K and pressure of 25 GPa. Seeding the system with a triplet-state ethyne molecule allowed the polymerization to be initiated already at a pressure of 9 GPa, which is in good agreement with experimental observations.

COMPUTATIONAL DETAILS

The reaction pathway of the polymerization of S_2N_2 has been simulated with *ab initio* Born−Oppenheimer molecular dynamics (MD) as implemented in CP2K-program[29] QUICKSTEP.[30] The crystal structure of β-S_2N_2[13] was used as a starting point in the simulation. Two supercells were considered: The smaller supercell is 2 × 2 × 1 (with respect to the unit cell axis *a*, *b*, and *c* of S_2N_2) and is called as the *221* supercell. The larger model uses the 4 × 4 × 2 supercell and is called as the *442* supercell. The *221* supercell contains eight S_2N_2 molecules and the larger *442* supercell contains 64 S_2N_2 molecules. The supercells were optimized before starting the actual MD simulations.

Calculations were performed with the revPBE[31,32] density functional using the molecular optimized short-range DZVP (DZVP-MOLOPT-SR)[33] basis set combined with the GTH[34,35] pseudopotentials.

The revPBE functional was chosen as a generally well-performing and efficient functional from the short list of functionals available in the CP2K library.[36] Molecular optimized (MOLOPT) basis sets have generally been found to perform better than similarly sized or slightly larger basis sets. The DZVP-MOLOPT reduces errors by a factor of 3−4 compared to the equivalent DZVP basis set.[33] The DZVP-MOLOPT basis set also exhibits a lower basis set superposition error (BSSE) than the comparable traditional basis sets. The short-range (SR) version of the basis has been constructed by removing the two highest exponent primitives resulting in slight increase in BSSE and significant improvement in speed. The basis set (DZVP-MOLOPT-SR) has been used as implemented in CP2K.

Grimme's DFT-D3[37] dispersion corrections were incorporated in the computations. The CSVR thermostat was used with the time step of 100.0 fs. The NVT ensemble was selected for the MD runs. Cut-off for planewaves was 350 Ry. Simulations were performed as cell optimization with 50 MD steps per cell optimization cycle with the time step of 4.0 fs.

A further set of simulations involved CASTEP[39] computations, which were performed on the *221* supercell without dynamics. Instead, the cell parameters and atom positions were optimized at incrementally higher pressures. The computations were carried out using the PBE[38] density functional with Grimme's DFT-D2[40] corrections. Norm-conserving planewaves with the 1000 eV cutoff and the *k*-point grid density of 0.04 1/Å were employed in the calculations. The *k*-point grid quality was maintained throughout the pressure compression and the consequent volume decrease (the 3 × 4 × 3 grid at the low pressure in the beginning of compression and the 7 × 5 × 3 grid at the high pressure end point).

Chemcraft,[41] Diamond,[42] VMD,[43] and Gnuplot[44] programs were used for the visualization of data.

RESULTS

General. It is well-established experimentally that at room temperature the polymerization of S_2N_2 is very slow and takes several hours or even days for completion.[1−5] The present *ab Initio* MD Born−Oppenheimer simulations were performed at high pressures and temperatures to speed up the reaction.

***221* Supercell.** The molecular dynamics simulations on the *221* supercell were performed at 300 K allowing for the optimization of all cell parameters. Each cell optimization step was preceded with 50 MD steps with a time step of 4.0 fs. The applied external pressure and potential energy profiles as a function of the simulation time are shown in Figure 2. It can be seen that the application of external pressure at 4.0, 8.0, and 12.0 ps results in incremental increases in energy. The reactions start to take place at the pressure of 25 GPa. There are several alternative routes for the polymerization of S_2N_2 rings, as exemplified in Figure 1. As the polymerization proceeds, energy drops rapidly. At the completion of the reaction, the simulation

dx.doi.org/10.1021/ic400273p | *Inorg. Chem.* 2013, 52, 4648−4657

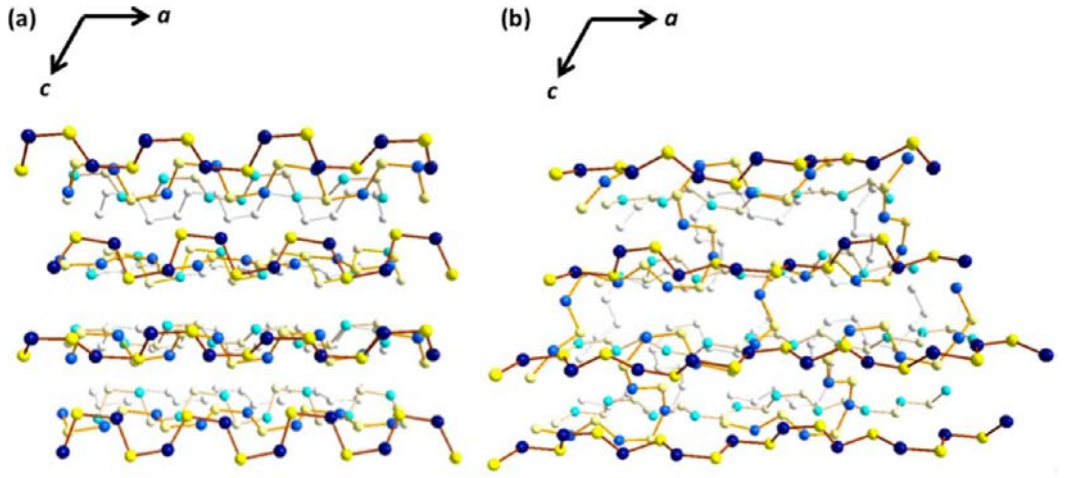

Figure 3. Simulated formation of the $(SN)_x$ polymer at 25 GPa and 300 K involving the *221* supercell. (a) Polymerization of S_2N_2 along *a* axis following the energy surface shown in Figure 2a. (b) Polymerization of S_2N_2 in other directions than solely along *a* axis creates a complicated network of crisscrossing $(SN)_x$ polymer chains. The energy surface is shown in Figure 2b. Sulfur atoms are indicated by yellow spheres and nitrogen atoms by blue spheres.

Scheme 2. Example of an Alternative Polymerization Pathway for the S_2N_2 Polymerization

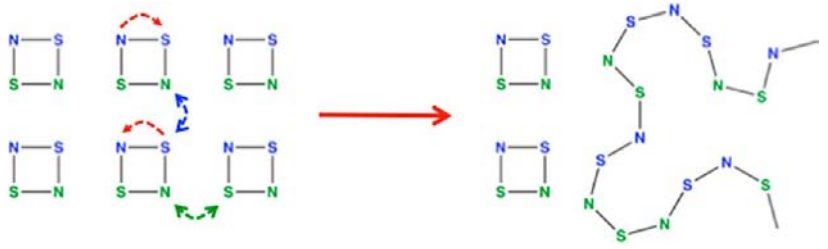

is allowed to relax for 10 ps. After this the pressure is incrementally lowered back to 0 GPa.

The energetically most favorable route of the polymer formation takes place at 31−34 ps after the start of the simulation [see Figure 2a], proceeds along *a* axis, and leads to the formation of zigzag chains of $(SN)_x$ polymers, as shown in Figure 3a. The polymerization is initiated by the approach of sulfur and nitrogen atoms of two adjacent rings that can oscillate about the nominal C_2 axis, which is perpendicular to the plane of the molecule. This leads to ring-opening and the propagation of the polymerization along the direction of *a* axis (see Scheme 1).

The rotation of the S_2N_2 ring facilitates the polymerization in other directions than along the *a* axis direction, as exemplified in Scheme 2. Consequently, the simulation on the *221* supercell often created complicated networks of criss-crossing polymer strands as shown in Figure 3b. Though the overall energy change is less favorable than in the linear polymer formation along *a* axis (see Figure 2b), the repeated simulations on the small *221* supercell have shown that the pathway depicted in Scheme 2 takes place more often than that shown in Scheme 1.

The effect of the excitation of S_2N_2 ring molecules to a triplet state prior to polymerization was also tested by the CP2K simulations on the *221* supercell. Excitation of S_2N_2 ring molecules to a triplet state prior to the polymerization allowed a single polymer chain to form along *a* axis already at 15 GPa pressure. Other rows of S_2N_2 rings in the *221* supercell remained unchanged.

The compression of the simulation supercell may cause bias on the reaction pathway. The effect of the directionality of the pressure on polymerization was tested by compressing the *221* supercell anisotropically in the directions *a*, *b*, *c*, *ab*, *ac*, and *bc* (the last three refer to two favored directions). The pressure in the favored direction was twice that in the other directions. Anisotropic testing was done at 300 K with stepwise pressure increases until the reaction was observed. Total simulation times varied from 22 to 72 ps depending on final pressures reached. The results are shown in Table 1.

Table 1. Effect of the Anisotropic Compression of the *221* Supercell

	pressure along axis (GPa)[a]			
favored direction	*a*	*b*	*c*	result
a	30	15	15	polymers along *a*
b	35	70	35	"metallic"
c	25	25	50	cross-linked polymer
bc	15	30	30	cross-linked polymer
ac	30	15	30	polymers along *a*
ab	40	40	20	polymers along *a*

[a]The final pressure during which the reaction was observed.

It can be seen from Table 1 that the enhanced compressions involving *a* axis directions result in polymers propagating along *a* axis. All enhanced compressions along the *c* axis but not involving the *a* axis lead to a complicated polymer network propagating roughly in the direction −101. The compression along the *b* axis does not result in polymerization, until at very high temperatures the atoms form a quasi-close-packed array and the system becomes formally metallic. It can be concluded

dx.doi.org/10.1021/ic400273p | *Inorg. Chem.* 2013, 52, 4648−4657

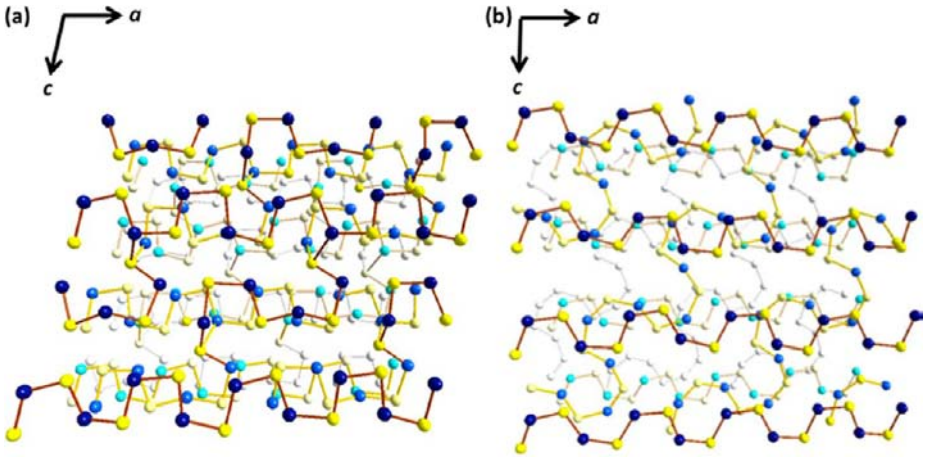

Figure 4. (a) After the polymerization at 57 GPa and 300 K, 50% of the S_2N_2 rings have formed single-strand polymer chains along the *a* axis. The other 50% are converted to polymers having cross-links with neighboring chains. (b) Upon lowering the external pressure to 0 GPa, the cross-linked polymers are converted to formally single-strand polymers propagating in the −101 direction. Sulfur atoms are indicated by yellow spheres and nitrogen atoms by blue spheres.

that isotropic compression itself does not favor any particular direction in reactivity and the polymer formation along *a* axis is energetically the most favorable pathway. While polymer formation involving the *c* axis direction is also possible, all polymer chains, which are formed, are confined in planes that are parallel to the *ac* planes.

It is likely that the MD simulations on the *221* supercell suffer from insufficient representation of the *k*-point grid, which in the CP2K MD simulations presented here is limited to the *γ*-point. Therefore, computational bias might affect the simulation results. The CASTEP computations on the same supercell include sufficiently high *k*-point grid for adequate modeling of intermolecular interactions. The use of *442* supercell also compensates for this with larger simulation space.

The CASTEP computations were performed without dynamics. Instead, the simulation cell parameters and atomic coordinates were optimized at incrementally higher pressures. Without dynamics the computations followed the lowest energy pathways, and no cross-linking was observed. Lack of dynamics required incremental increase of pressure until 80 GPa when the system polymerized along the *a* axis leading to a lattice, which is similar to that shown in Figure 3a.

***442* Supercell.** Two sets of simulations were performed on the *442* supercell. The first set was performed at 300 K by increasing the pressure rapidly at 4 ps intervals until a reaction was observed at 57 GPa. After the initiation, the polymerization rapidly progressed to completion. Upon lowering the external pressure, the compressed polymer relaxed to the end-product. Both the compressed polymer and the relaxed end-product are shown in Figure 4.

The polymerization proceeded simultaneously in both *a* and *b* axis directions, as the pressure was increased rapidly. Upon completion of the polymerization with the external pressure still at 57 GPa, 50% of the S_2N_2 molecules can be seen to have formed strands along the *a* axis (see Figure 4a). While the other 50% of the ring molecules have also polymerized along the *a* axis, there is significant cross-linking to neighboring chains. When the pressure was relaxed in the system, the cross-links connecting neighboring polymers in the *b* axis direction cleaved, and single-strand chains propagating in the direction along the *ac* plane were formed. The rest of the chains in the lattice remained directed in the *a* axis direction (see Figure 4b). This situation bears a qualitative resemblance to that computed for the smaller *221* supercell (see Figure 2b).

The fast pressure increase resulted in a high pressure of 57 GPa, before the polymerization was initiated. Upon reaching this threshold, the reaction proceeded very rapidly. This might explain the high propensity to cross-linking in the simulation. Therefore, another set of simulations was carried out on the *442* supercell by increasing the pressure more slowly, but also varying the temperature during the simulation. The pressure and temperature profiles are shown in Figure 5 together with the potential energy evolution.

After increasing the pressure in 5 and 10 GPa increments at 300 K in 4 ps intervals until 35 GPa was reached, the temperature of the system was raised up to 600 K. The simulation was continued at 35 GPa for 34 ps after which the

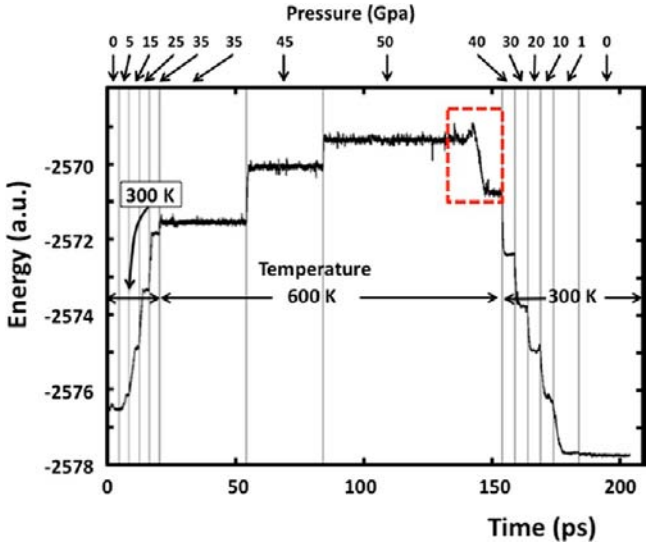

Figure 5. Potential energy evolution during the $S_2N_2 \rightarrow (SN)_x$ polymerization simulated on the *442* supercell. Vertical lines designate the times where pressure is changed in the simulation. The temperatures during the simulation are also indicated in the figure. The time period during which the polymerization of S_2N_2 took place is indicated by a red dashed rectangle.

dx.doi.org/10.1021/ic400273p | *Inorg. Chem.* 2013, 52, 4648−4657

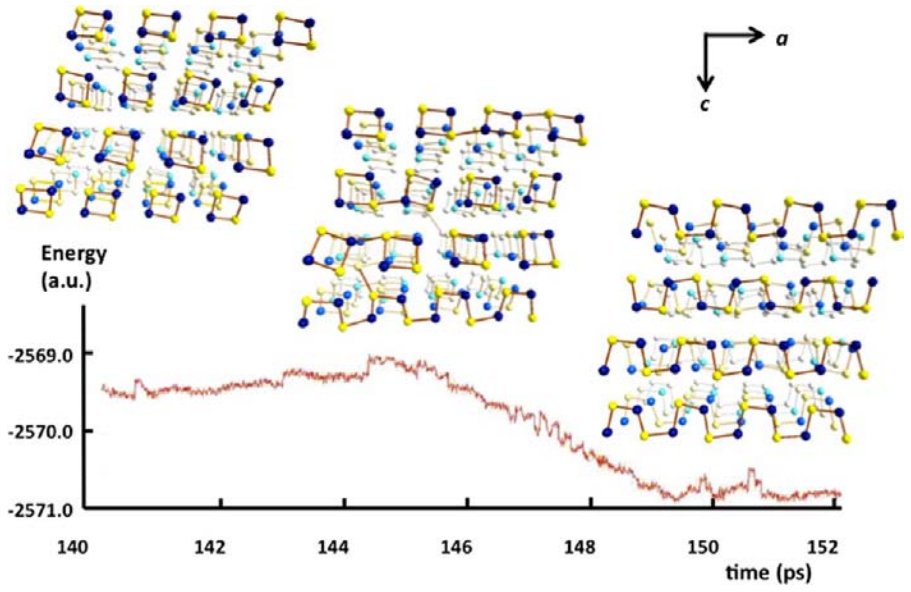

Figure 6. Energy profile of the polymerization of S_2N_2 rings to $(SN)_x$ at 50 GPa and 600 K (the time is given from the beginning of the simulation; see Figure 5). Sulfur atoms are indicated by yellow spheres and nitrogen atoms by blue spheres (*b* axis is directed away from the reader).

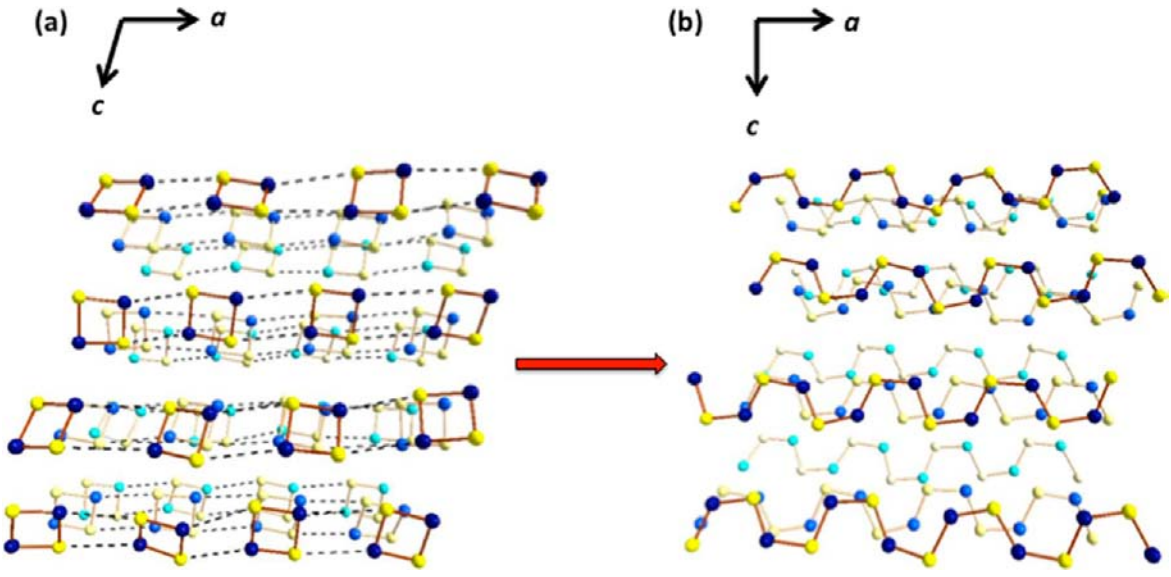

Figure 7. Solid state lattices of (a) initial S_2N_2 rings and (b) final $(SN)_x$ chains in the simulated *442* supercell at 300 K and 0 GPa. Sulfur atoms are indicated by yellow spheres and nitrogen atoms by blue spheres. The *b* axis in both parts a and b are directed away from the reader.

pressure increases to 45 and 50 GPa were conducted at intervals of 30 ps. The peak pressure of 50 GPa was maintained for 70 ps during which time the polymerization was observed. The pressure was subsequently lowered back to 0 GPa in 1 or 10 GPa decrements.

Polymerization was observed at 50 GPa and 600 K in the time interval 143−152 ps, as indicated by a red-dashed rectangle in Figure 5. The process is shown in more detail in Figure 6. Prior to the actual polymerization, the S_2N_2 rings interact with each other resulting in the rapid formation and dissociation of short-lived larger assemblies. The polymerization proceeds along the *a* axis but with the formation of instantaneous cross-links. These cross-linked networks eventually revert to the single-strand $(SN)_x$ polymeric chains with a consequent fall in total energy. An animated clip of the polymerization process is shown in Supporting Information.

After the completion of polymerization, no further change was observed upon lowering the external pressure back to 0 GPa apart from the slight alteration of the packing of the chains in the lattice. The simulated solid state lattices of initial S_2N_2 and final $(SN)_x$ in the *442* supercell are shown in in Figure 7.

It is interesting to note that the simulation with slower pressure variation resulted only in the formation of parallel polymeric chains with no indication of cross-linking in the final structure. The lattice resembles qualitatively the experimental crystal lattice.[6,7,13] However, the zigzag orientation of the polymers in the simulated *442* supercell is more random, while that in the experimental structure crystallizes with higher long-range order (compare the lattices of the experimental and simulated crystal structures of $(SN)_x$ in Figures 1b and 7b). Since there are two energetically equal ways that the adjacent rings can approach each other and cleave (see Scheme 1), it is

dx.doi.org/10.1021/ic400273p | *Inorg. Chem.* 2013, 52, 4648−4657

Scheme 3. Possible Slippage of Polymers with Respect to Each Other along the Direction of the Polymer Chain Can Create Ordered Structures of Higher Symmetry

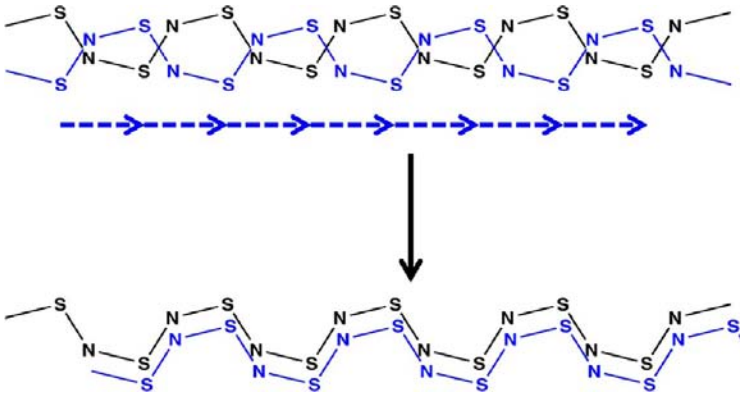

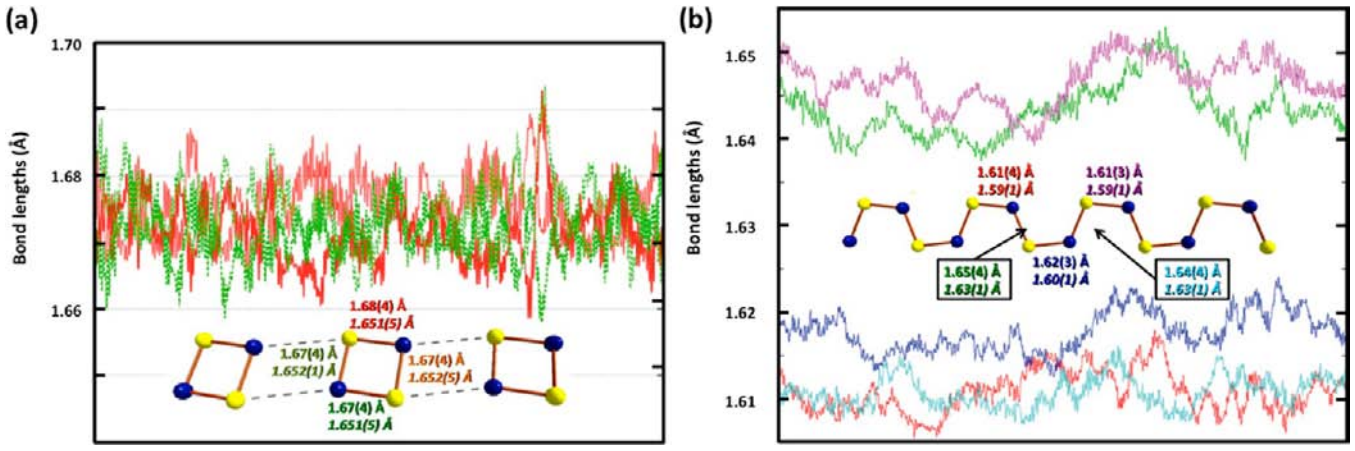

Figure 8. Simulated (300 K, 0 GPa) and experimental S−N bond lengths (Å) of (a) initial S_2N_2 and (b) relaxed $(SN)_x$ (sulfur atoms are indicated by yellow spheres and nitrogen by blue spheres). The variation of the metrical values is shown for 10 ps. The numerical values in the figure are color-coded to correspond to those of the plots. Their standard deviations have been calculated from the moving averages covering 50 cycles of simulation. The italicized values refer to those from the crystal structure determinations by Cohen et al.[13].

not surprising that in the simulations the neighboring chains do not show long-range order. Several attempts to determine the crystal structures of various polymorphs of $(SN)_x$ have indeed also indicated severe disorder,[3] and it has been possible to establish that $(SN)_x$ crystallizes in ordered chains in the lattice only in some cases.[7,13] The change in the lattice symmetry upon polymerization and the lack of long-range coherence with consequent twinning have been discussed by Cohen et al.[13] Our simulated lattice with disordered chains could in principle be converted to the more ordered stacking by allowing the neighboring chains to slide with respect to each other and finally assume a higher order (see Scheme 3).

In order to get an approximate estimate of energy barrier to the slippage shown in Scheme 3, we performed DFT computations by moving one chain with respect to its neighbors in the *442* supercell. The energy barrier turned out to be *ca.* 75 kJ mol^{-1} and could be low enough to allow random packing in the high pressures and temperatures prevailing during the simulations. It is possible that, despite Grimme's correction for dispersion,[37] the intermolecular interactions in the actual crystal structure are stronger than those computed in the simulated lattice leading to more favorable relative energy for the ordered packing of polymer chains.

The simulated average S−N bond length of 1.67(4) Å in initial S_2N_2 (see Figure 8a for the variation of individual bond lengths at 300 K and 0 GPa during a time period of 10 ps) is in good agreement with the bond length of 1.653(5) Å[13] determined by X-ray diffraction. Due to the oscillation of the molecules about their equivalent lattice positions during the MD simulation, the computed instantaneous in-plane intermolecular S···N contacts vary between 2.68 and 3.41 Å [average 3.0(2) Å], and the out-of-plane contacts span a range 2.86−3.88 Å [average 3.3(2) Å]. These values are also in agreement with the in-plane and out-of-plane close contacts of 2.868(5) and 3.474(5) Å, which have been observed in the crystal lattice.[13] The simulated average S−N bond lengths in $(SN)_x$ (300 K, 0 GPa) alternate 1.61(4) and 1.65(4) Å and are also in good agreement with those determined experimentally by X-ray diffraction (see Figure 8b). The simulated bond angles in both S_2N_2 and $(SN)_x$ also agree with experimental values.

Possible reaction activation by exciting starting S_2N_2 molecules into the triplet-state in the *442* supercell was tested in a similar fashion as was done in the case of the smaller *221* supercell. In this case, the triplet molecules were introduced into the simulation at 45 GPa and 600 K using the compressed S_2N_2 structure from the previous *442* simulation, which by that stage had involved only singlet molecules. After another 10 ps simulation at 45 GPa, the pressure was increased to 50 GPa, after which the system rapidly polymerized in a similar fashion, as was observed in the case of the singlet model (see Figure 7).

dx.doi.org/10.1021/ic400273p | *Inorg. Chem.* 2013, 52, 4648−4657

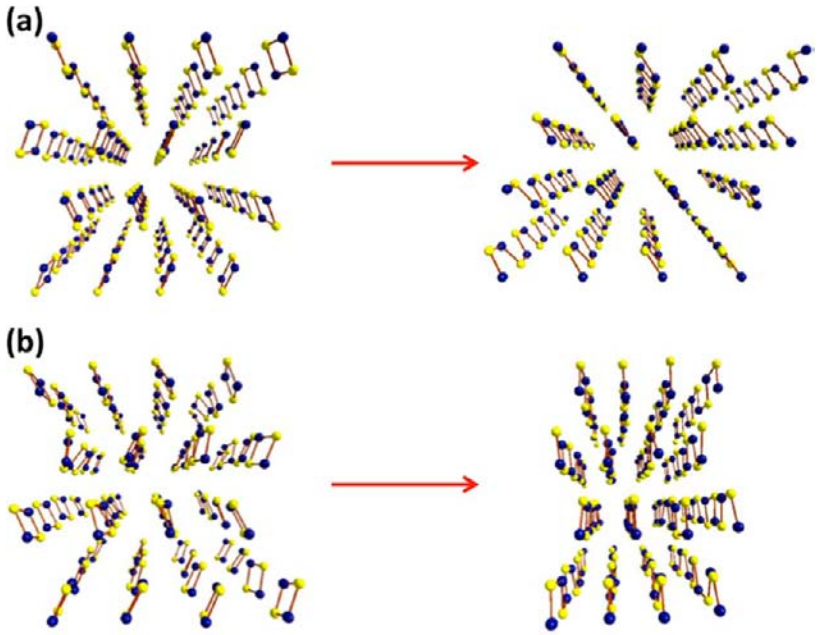

Figure 9. Orientation of the molecular planes of the starting S_2N_2 and final polymeric $(SN)_x$. (a) Experimental crystal structures.[13] (b) Solid-state simulations on the *442* supercell.

The main difference compared to the singlet model was the displacement of one of the sulfur atoms from the chain lattice due to persistent side reactions.

Another triplet simulation was performed at 300 K. Like before, the simulation was started with 10 ps period at 45 GPa followed by another 10 ps at 50 GPa pressure. After this the pressure was increased to 52.5 GPa. The reaction was observed after 5 ps simulation at this pressure. The polymerization proceeded very cleanly with practically no side reactions. The lower simulation temperature also most likely favored cleaner reaction compared to that at 600 K.

The triplet simulations seem to activate after shorter simulations, but do not show any other significant qualitative differences to the singlet simulations.

DISCUSSION

The formation of the $(SN)_x$ polymer from S_2N_2 indeed seems to follow ring cleavage involving the minimized root-mean-square displacements of the atoms.[16−19] Our solid-state simulations indicate only a minor tendency toward ring puckering with short-lived side reactions and no persistent polymerization perpendicular to the plane of the S_2N_2 molecules, which has recently been proposed on the basis of gas-phase computations of singlet and triplet electronic states of molecular S_2N_2.[20] While the simulations led to the formation of short-lived cross-links between the neighboring chains in *b* axis directions during the polymerization process, the relaxed final polymers showed no bonds in *b* axis direction under any conditions.

The energetically most favorable polymer formation propagated along the *a* axis in both *221* and *442* simulation supercells. The oscillation of the S_2N_2 rings about the C_2 axis perpendicular to the plane of the molecule allows the sulfur and nitrogen atoms to approach each other. The animated simulation on the *442* supercell (see Supporting Information) indicates that the cleavage of a bond in the S_2N_2 ring and the formation of a bond with the neighboring ring molecule take place virtually simultaneously. However, since ESR signals have been observed during the reactions but not in the starting materials or end products,[13,23] it is likely that ring-opening precedes the polymer formation.

The same C_2 oscillation of the S_2N_2 molecules may also lead to the polymer formation in the direction of the *c* axis, which persists also when the external pressure has been lowered back to 0 GPa. This may result in the complicated network of polymer chains, which is observed in many simulations involving the *221* supercell as well as in those involving the *442* supercell with a fast pressure increase (see Figures 3b and 4b, respectively). In simulations on the *442* supercell, which involved slower pressure variations, such cross-links were short-lived and the final polymer lattice consisted of only parallel $(SN)_x$ chains. It is probable that the formation of such complicated polymer networks is the cause of the several disordered polymorphs of $(SN)_x$.[3]

The introduction of the triplet-state wave function of S_2N_2 into our MD calculations on both supercells resulted in the initiation of the polymerization at lower pressures than when only singlet starting rings were involved. These polymerizations also seemed to proceed more cleanly along *a* axis. Otherwise, the simulations of reactions involving both singlet and triplet S_2N_2 proceeded in a similar fashion. The triplet state of S_2N_2, however, lies significantly above the single ground state. The comprehensive triplet surface mapping by Mawhinney and Goddard places the triplet state about 200 kJ mol^{-1} above the singlet ground state[20] in agreement with other computational and experimental studies.[3] It should be noted, however, that the high excitation energy is consistent with the measured activation energy of 172 kJ mol^{-1} for the polymerization.[21,22]

Müller et al.[7] have discussed the polymer formation based on time-resolved X-ray powder diffraction study involving Rietveld refinement. According to their conclusions, every second layer of the S_2N_2 rows in the herringbone packing shown in Figure 9a will undergo a shear prior to the polymerization rendering all molecules in the lattice parallel. The subsequent polymerization

dx.doi.org/10.1021/ic400273p | *Inorg. Chem.* 2013, 52, 4648−4657

creates a $(SN)_x$ lattice in which the planes of all polymer chains are parallel, as also shown in Figure 9a.

We did not observe such packing changes of the S_2N_2 molecules through shear transformations. The S_2N_2 rings seemed to show no apparent energetic benefits from adopting a different packing prior to the polymerization. Such tendencies have not been observed in any of the simulations. If the shear transformation were energetically or entropically achievable, such packing alteration should have a relatively low energy barrier and a precursor structure of S_2N_2 would be expected to be formed in the simulations. This does not seem to be the case. Furthermore, if the planes of all S_2N_2 ring molecules were to become parallel to the *ac*-plane prior to the polymerization, both the *a* and the *c* axis directions would be equally likely for polymerization and would result in more severe disorder than what has been observed experimentally.

However, there is a related change in the directions of the molecular planes between the initial S_2N_2 and final relaxed $(SN)_x$, the lattices of which have been simulated at 300 K and 0 GPa (see Figure 9b). The reorientation takes place simultaneously during the polymerization (see the animation in Supporting Information). The changes in the packing may destabilize the cross-links in favor of the parallel chains along *a* axis.

The current simulations involved supercells of two different sizes. The *221* supercell is computationally more accessible, but the simulation space is probably too small for reliable results. The *442* supercell, on the other hand, seems to yield chemically reliable information, but is computationally much more demanding. It can be noted that qualitatively both supercells yielded similar results, though the polymerization in the smaller *221* supercell was initiated at a lower pressure than when the simulation was carried out on the larger *442* supercell. The MD calculations on both the *221* and *442* supercells, as well as the CASTEP calculation involving the *221* supercell, all yielded an estimate close to -50 kJ mol^{-1} for the polymerization of one mole of S_2N_2 [CP2K(*221*) -50 kJ mol^{-1}; CP2K(*442*) -49 kJ mol^{-1}; CASTEP(*221*) -48 kJ mol^{-1}].

The conditions during the MD simulation of the polymerization differ significantly from those during the actual experiment. The conversion of the S_2N_2 single crystal into a $(SN)_x$ single crystal takes place at room temperature or at slightly elevated temperature, but takes hours for completion.[1−5] While the temperature in the simulations is comparable to that in the experiment, the pressure needed for the reaction to occur at the picosecond time-scale is very high. It is therefore not self-evident that the MD results at high pressure bear a direct relationship to the experimental observations. However, the polymerization is consistent with the minimized root-mean-square displacements of the atoms.[16−19] It is possible that the triplet S_2N_2 plays a more significant role at ambient pressure.

While the pressures used in simulations are very high, experimental measurements on the superconductivity of the polymer structure suggest that the material remains intact at least to 40 GPa pressure.[45] This suggests that, in principle, the simulation conditions would not be too extreme, although direct comparison between experimental and theoretical pressure values cannot be made.

The final relaxed structure for the MD simulation on the *442* cell and CASTEP simulation for the *221* correspond on qualitative level to available experimental data. The layered chain packing resembles the experimental structure.

CONCLUSIONS

In this contribution we have presented the first molecular dynamics simulation of the solid-state topochemical polymerization S_2N_2 to $(SN)_x$ by involving DFT methods and periodic functions. High pressures and slightly elevated temperatures have been used to lower the activation barriers and to increase the rate of the reaction. The simulations have been performed both on the *221* and *442* supercells.

As the external pressure in the simulation is raised to a given threshold (25 and 50 GPa in case of the *221* and *442* supercells, respectively), the polymer formation is initiated by the cleavage of one bond in one of the S_2N_2 molecules with a virtually instantaneous attack of the acyclic fragment thus formed on the neighboring ring molecule. The energetically most-favored reaction then quickly propagates along the *a* axis throughout the lattice. The structures of the polymer chains are in good agreement with that observed experimentally in the crystal structure, but there is less long-range order between the neighboring chains. It is conceivable that at high pressures and elevated temperatures such slippage takes place more easily than at ambient pressure and pressure thus causing more disorder in the simulations.

Upon polymerization the packing of the molecules changes from the herringbone structure of the S_2N_2 lattice to the layered structure in the $(SN)_x$ lattice. While the simulated final lattice of the polymer differs from that observed experimentally, the simulated and experimental packing changes bear a qualitative similarity.

During the simulations, the polymerization has also been observed to propagate along the *c* axis in addition to the *a* axis, but these side reactions generally disappear toward the end of the simulations. In the case of the smaller *221* supercell and also that of the *442* supercell involving fast pressure increases, the polymers propagating in both *a* and *c* axis directions persisted at the end of the reaction, and the polymer was a complicated network of sulfur−nitrogen chains. Such networks might be a computational artifact, but may also find experimental support in the observation of several polymorphs $(SN)_x$ with disorder in the lattice.

ASSOCIATED CONTENT

Supporting Information

Animated clip of the polymerization process of S_2N_2 to $(SN)_x$ at 600 K and 50 GPa involving the *442* supercell. This material is available free of charge via the Internet at http://pubs.acs.org.

AUTHOR INFORMATION

Corresponding Author

*E-mail: risto.laitinen@oulu.fi. Phone: (35840) 5056111. Fax: (3588) 553-1608.

Notes

The authors declare no competing financial interest.

ACKNOWLEDGMENTS

We are grateful to Prof. Tristram Chivers for helpful discussions. Financial support from the Academy of Finland is gratefully acknowledged. We also thank Finnish CSC−IT Center for Science Ltd. for their generous provision of computational resources.

REFERENCES

(1) Greene, R. L.; Street, G. B.; Suter, L. J. *Phys. Rev. Lett.* **1975**, *34*, 577−579.
(2) Labes, M. M.; Love, P.; Nichols, L. F. *Chem. Rev.* **1979**, *79*, 1−15.
(3) Banister, A. J.; Gorrell, I. B. *Adv. Mater.* **1998**, *10*, 1415−1429.
(4) Chivers, T. *A Guide to Chalcogen-Nitrogen Chemistry*; World Scientific Publishing Co, Inc.: Singapore, 2005; p 340.
(5) Chivers, T.; Laitinen, R. S. In *Handbook of Chalcogen Chemistry*, Devillanova, F., Ed.; RSC Publishing: London, 2007; pp 223−285.
(6) Mikulski, C. M.; Russo, P. J.; Soran, M. S.; MacDiarmid, A. G.; Garito, A. F.; Heeger, A. J. *J. Am. Chem. Soc.* **1975**, *97*, 6358−6363.
(7) Müller, H.; Svensson, S. O.; Birch, J.; Kvick, Å. *Inorg. Chem.* **1997**, *36*, 1488−1494.
(8) Passmore, J.; Rao, M. N. S. *J. Chem. Soc., Chem. Commun.* **1980**, 1268−1269.
(9) Kennett, F. A.; MacLean, G. K.; Passmore, J.; Rao, M. N. S. *J. Chem. Soc., Dalton Trans.* **1982**, 851−857.
(10) Love, P.; Kao, H. I.; Myer, G. H.; Labes, M. M. *J. Chem. Soc., Chem. Commun.* **1978**, 301−302.
(11) Banister, A. J.; Hauptman, Z. V.; Rawson, J. M.; Wait, J. T. *J. Mater. Chem.* **1996**, *6*, 1161−1164.
(12) King, R. S. P.; Kelly, P. F.; Dann, S. E.; Mortimer, R. J. *Chem. Commun.* **2007**, 4812−4814.
(13) Cohen, M. J.; Garito, A. F.; Heeger, A. J.; MacDiarmid, A. G.; Mikulski, C. M.; Saran, M. S.; Kleppinger, J. *J. Am. Chem. Soc.* **1976**, *98*, 3844−3848.
(14) Kelly, P. F.; King, R. P. S.; Mortimer, R. J. *Chem. Commun.* **2008**, 6111−6113.
(15) Bleay, S. M.; Kelly, P. F.; King, R. S. P. *J. Mater. Chem.* **2010**, *20*, 10100−10102.
(16) Baughman, R. H.; Chance, R. R.; Cohen, M. J. *J. Chem. Phys.* **1976**, *64*, 1869−1876.
(17) Baughman, R. H.; Chance, R. R. *J. Polym. Sci., Polym. Phys. Ed.* **1976**, *14*, 2019−2035.
(18) Baughman, R. H.; Apgar, P. A.; Chance, R. R.; MacDiarmid, A. G.; Garito, A. F. *J. Chem. Phys.* **1977**, *66*, 401−409.
(19) Young, R. J.; Baughman, R. H. *J. Mater. Sci.* **1978**, *13*, 55−61.
(20) Mawhinney, R. C.; Goddard, J. D. *Inorg. Chem.* **2003**, *42*, 6323−6337.
(21) Kanazawa, H.; Stejny, J.; Keller, A. *J. Mater. Sci.* **1990**, *25*, 3838−3842.
(22) Kanazawa, H.; Stejny, J.; Keller, A. *J. Mater. Sci.* **1991**, *26*, 1635−1639.
(23) Love, P.; Labes, M. M. *J. Chem. Phys.* **1979**, *70*, 5147.
(24) Hemley, R. J. *Annu. Rev. Phys. Chem.* **2000**, *51*, 763−800.
(25) Schettino, V.; Bini, R. *Phys. Chem. Chem. Phys.* **2003**, *5*, 1951−1965.
(26) Schettino, V.; Bini, R.; Ceppatelli, M.; Citroni, M. *Phys. Scr.* **2008**, *78*, 058104−5.
(27) Sakashita, M.; Yamawaki, H.; Aoki, K. *J. Phys. Chem.* **1996**, *100*, 9943−9947.
(28) Bernasconi, M.; Chiarotti, G. L.; Focher, P.; Parrinello, M.; Tosatti, E. *Phys. Rev. Lett.* **1997**, *78*, 2008−2011.
(29) *CP2K version 2.1.369 (Development Version)*; CP2K Developers Group, 2010. CP2K is freely available from http://www.cp2k.org/
(30) VandeVondele, J.; Krack, M.; Mohamed, F.; Parrinello, M.; Chassaing, T.; Hutter, J. *Comput. Phys. Commun.* **2005**, *167*, 103−128.
(31) Perdew, J. P.; Burke, K.; Ernzerhof, M. *Phys. Rev. Lett.* **1996**, *77*, 3865−3868.
(32) Zhang, Y.; Yang, W. *Phys. Rev. Lett.* **1998**, *80*, 890.
(33) VandeVondele, J.; Hutter, J. *J. Chem. Phys.* **2007**, *127*, 114105−9.
(34) Goedecker, S.; Teter, M.; Hutter, J. *Phys. Rev. B* **1996**, *54*, 1703−1710.
(35) Hartwigsen, C.; Goedecker, S.; Hutter, J. *Phys. Rev. B* **1998**, *58*, 3641−3662.
(36) Yang, K.; Zheng, J.; Zhao, Y.; Truhlar, D. G. *J. Phys. Chem.* **2010**, *132*, 164117−10.
(37) Grimme, S.; Antony, J.; Ehrlich, S.; Krieg, H. *J. Chem. Phys.* **2010**, *132*, 154104−19.
(38) Clark, S. J.; Segall, M. D.; Pickard, C. J.; Hasnip, P. J.; Probert, M. J.; Refson, K.; Payne, M. C. *Z. Kristallogr.* **2005**, *220*, 567−570.
(39) Perdew, J. P.; Burke, K.; Ernzerhof, M. *Phys. Rev. Lett.* **1996**, *77*, 3865−3868.
(40) Grimme, S. *J. Comput. Chem.* **2006**, *27*, 1787−1799.
(41) http://www.chemcraftprog.com (v1.6 build 350).
(42) *Diamond 3.2h—Crystal and Molecular Structure Visualization Crystal Impact*; K. Brandenburg and H. Putz GbR: Bonn.
(43) Humphrey, W.; Dalke, A.; Schulten, K. *J. Mol. Graphics* **1996**, *14*, 33−38 , VMD version 1.9.
(44) Williams, T.; Kelley, C. *Gnuplot 4.4 patchlevel 3: An Interactive Plotting Program*; 2011, http://gnuplot.sourceforge.net/.
(45) Dunn, K. J.; Bundy, F. P.; Interrante, L. V. *Phys. Rev. B* **1981**, *23*, 106−111.